Smart Structures and Systems, *Vol. 25, No. 2 (2020) 169-181*
DOI: https://doi.org/10.12989/sss.2020.25.2.169

Optimal sensor placement for bridge damage detection using deflection influence line

Chengyin Liu [a], Jun Teng [b] and Zhen Peng*

Department of Civil and Environment Engineering, Harbin Institute of Technology, Shenzhen, China

(*Received March 11, 2019, Revised July 18, 2019, Accepted October 13, 2019*)

Abstract. Sensor placement is a crucial aspect of bridge health monitoring (BHM) dedicated to accurately estimate and locate structural damages. In addressing this goal, a sensor placement framework based on the deflection influence line (DIL) analysis is here proposed, for the optimal design of damage detection-oriented BHM system. In order to improve damage detection accuracy, we explore the change of global stiffness matrix, damage coefficient matrix and DIL vector caused by structural damage, and thus develop a novel sensor placement framework based on the Fisher information matrix. Our approach seeks to determine the contribution of each sensing node to damage detection, and adopts a distance correction coefficient to eliminate the information redundancy among sensors. The proposed damage detection-oriented optimal sensor placement (OSP) method is verified by two examples: (1) a numerically simulated three-span continuous beam, and (2) the Pinghu bridge which has existing real damage conditions. These two examples verify the performance of the distance corrected damage sensitivity of influence line (DSIL) method in significantly higher contribution to damage detection and lower information redundancy, and demonstrate the proposed OSP framework can be potentially employed in BHM practices.

Keywords: bridge health monitoring; deflection influence line; damage detection; sensitivity analysis; distance coefficient correction

1. Introduction

Structural health monitoring (SHM) techniques have gained considerable attention in bridge structures for ensuring their functionality and safety during their long service life. Damage detection is unarguably one of the most important aspects of SHM. Identifying the presence of the damage (structural or material change that affects the behavior of the structure adversely) might be considered as the first step to take preventive actions and to start the process towards understanding the root causes of the problem (Flaga and Furtak 2015, Mao *et al.* 2018). Therefore, the capability of any SHM system for estimating the existence, location and extent of damage is an essential issue. In this context, reasonable sensor deployment that sensitive to structural damage whereas insensitive to environmental disturbance becomes an essential consideration.

In order to improve damage detection accuracy, sensors should be placed on locations with higher sensitivity and contribution to damage detection (Chang and Pakzad 2014). In the past few decades, quite a few vibration-based sensor placement methods have been proposed. Some of these methods can be found in literature and the references therein (Pei *et al*. 2018, Li *et al.* 2017, Talebpour and Mahmassani 2016, Kong *et al*. 2014, Jin *et al*. 2015, Kammer and Brillhart 2013). These methods can be generally categorized into two categories: the modal feature-oriented and the damage detection-oriented.

Modal feature-oriented sensor placement methods examine the information on sensing nodes that are sufficiently sensitive to detect changes in modal parameters. Although modal parameters are among the early features considered for damage detection, they have proved to be not the most effective damage features, considering they are not sensitive to local damage and easily affected by environmental factors (Soman *et al*. 2017, Chang and Pakzad 2014, Kammer and Brillhart 2013). Regarding OSP for damage detection, most of the limited works published deal with this issue as a parameter identification task (Talebpour and Mahmassani 2016). One of the first and most well-established approaches was the maximization of a norm of the Fisher Information Matrix (FIM). In Xia and Hao (2000), a residual vector was obtained and its sensitivity to structural damage as well as the measurement noise were analyzed. The authors selected those sensing nodes sensitive to residual vector while insensitive to environmental noise as a sensor deployment strategy. Shi *et al.* (2000) developed a damage sensitivity matrix to form FIM, and defined a contribution matrix $\boldsymbol{E}$ to calculate the contribution value of each node to damage detection. However, the inverse matrix of FIM which is crucial to establish contribution matrix $\boldsymbol{E}$ is not easy to obtain. To this end, Liu *et al.* (2013) in a recent study, defined the contribution of each sensing node by calculated the rank

*Corresponding author, Ph.D. Student,
E-mail: zhen.peng@postgrad.curtin.edu.au
[a] Associate Professor, E-mail: chengyin.liu@hit.edu.cn
[b] Professor, E-mail: tengj@hit.edu.cn

http://www.techno-press.org/?journal=sss&subpage=7
ISSN: 1738-1584 (Print), 1738-1991 (Online)

value of FIM instead of contribution matrix inversion. In their approach, generalized inverse matrix method and singular value decomposition method were adopted to reduce the singularity in reversing (Lee *et al*. 2010, Wang *et al*. 2005). Additionally, information redundancy problem is often seen in existing damage detection-oriented OSP, since the enrolled sensors may provide similar information to damage detection (Singh *et al*, 2016). Loutas and Bourikas (2017) proposed a two-stage method by removing the enrolled sensing nodes that close to each other in terms of geographical distribution. Similar approaches are followed in Refs (Schulte *et al*. 2006, Li *et al*. 2012).

Besides the vibration-based monitoring, deflection measurement using displacement sensor is another common issue in SHM especially for bridge structure bearing moving vehicle loads (Cho *et al.* 2018). Displacement recordings may be exploited for determining excessive loads during in-service conditions, as well as for quantifying regular operational loads (e.g., traffic) to serve as feedback in bridge design practice (Huang *et al*. 2016, Cavadas *et al*. 2013). Deflection responses of bridge are dominated by vehicle loads and may be less affected by environmental factors during the period of vehicle passing on the bridge (Wang and Ren 2017). DIL-based damage detection method offers valuable tools towards a comprehensive evaluation of bridge systems due to the curvature characteristics of DIL. Through analyzing the change of DIL measured by displacement sensors, structural damage can be detected (Hong *et al*. 2002, Štimac-Grandić 2014). In this respect, DIL could be an economical alternative to enhance damage-related information by extracting displacement responses on bridge critical sections under moving load.

A number of DIL-based methods have been proposed for bridge damage detection in literature. For instance, He *et al.* proposed a two-stage method with the ability to quantify structural damages by using the quasi-static moving load induced displacement response (He *et al*. 2013). Cavadas *et al*. (2013) discussed the application of data-driven methods on moving-load responses in order to detect the occurrence and the location of damage. Chen *et al.* (2017) derived the theoretical formulae of DIL before and after damage occurred, and prove that the difference of DIL and its first and second order partial derivatives can be used in damage localization. In their study, multiple damage locations can be determined using the mid-span deflection time history induced by moving loads. Nevertheless, these methods may still suffer from the lack of practicality since a large number of sensors are required to quantify damage extent. To the best of authors' knowledge, optimization of displacement sensors in lieu of DIL theory has rarely been studied in the literature.

In the present work, we develop a systematic DIL-based OSP framework for bridge damage detection. In our approach, displacement sensors are deployed in nodes with maximum contribution to damage detection, and the damage extent can be quantified accurately if deflection responses before and after damage occurred are available. In what follows, the principle of DIL based damage extent quantification method and OSP framework are introduced in Section 2. In Section 3, the procedure of OSP framework is illustrated and verified using two numerical examples: (1) a three-span continues beam model; (2) the Pinghu (PH) bridge, which has existing real damage conditions. Finally, Section 4 concludes this article and highlights our future work.

2. Methodology–Sensor placement

2.1 Bridge damage detection based on the analysis of DIL

The influence line is defined as the response of a structure at a certain measurable location to a unit load at an arbitrary location. Assuming that the structure behaves linearly and the dynamic response is negligible compared to the static response, it is possible to utilize the static influence line to generate the response of a structure. DIL can be calculated by placing a unit vertical force on the structure and selecting parts of degrees of freedom (DOFs) as output, namely

$$\boldsymbol{DIL} = \boldsymbol{SK}^{-1}\boldsymbol{Q} \tag{1}$$

where $\boldsymbol{K}^{-1}$ denote the baseline global flexibility matrix of order (n×n). $\boldsymbol{Q}$ and $\boldsymbol{S}$ denote the input forces selection matrix of order (n×m) and the output vertical displacement selection matrix of order (l×n), respectively. m, l and n are input, output DOFs and the overall DOFs, respectively. $\boldsymbol{Q}$ and $\boldsymbol{S}$ are defined as follows

$$\boldsymbol{Q} = \overbrace{\begin{bmatrix} \cdots & & & \cdots & & & \cdots \\ \cdots & 0 & & \cdots & & & \cdots \\ \cdots & 1 & & \cdots & & & \cdots \\ \cdots & 0 & 0 & \cdots & & & \cdots \\ \cdots & & 1 & \cdots & \vdots & \vdots & \cdots \\ \cdots & & 0 & \cdots & 0 & & \cdots \\ \cdots & \vdots & \vdots & \cdots & 1 & & \cdots \\ \cdots & & & \cdots & 0 & 0 & \cdots \\ \cdots & & & \cdots & & 1 & \cdots \\ \cdots & 0 & 0 & & & 0 & \cdots \end{bmatrix}}^{m} \begin{matrix} \\ horizontalDOF \\ verticalDOF \\ rotationDOF \\ n \\ \\ \\ \\ \\ \\ \end{matrix}, \qquad \boldsymbol{S} = \overbrace{\begin{bmatrix} 0 & \cdots & 1 & 0 & \cdots & 0 & & \cdots & 0 & & 0 \\ 0 & \cdots & 0 & & \cdots & 1 & 0 & \cdots & 0 & & 0 \\ 0 & \cdots & & & \cdots & & & \cdots & 1 & 0 & 0 \\ \vdots & \vdots & \vdots & \vdots & \vdots & \vdots & \vdots & \vdots & \vdots & \vdots & \vdots \end{bmatrix}}^{n} l \tag{2}$$

As illustrated in Eq. (1), DIL can be regarded as a sub-matrix of structural global flexibility matrix. Hence, analysis of the flexibility matrix is actually a useful tool for understanding how the DIL-based damage extent quantification method works.

Note that the stiffness matrix of i-th element $\boldsymbol{K}_i$ is usually rank deficiency. Assuming the rank of $\boldsymbol{K}_i$ is r, the eigen-decomposition of element stiffness matrix can be expressed as

$$\boldsymbol{K}_i = \boldsymbol{U}_i\boldsymbol{\Lambda}_i\boldsymbol{U}_i^T = \sum_{j=1}^{r}\sigma_i^j\boldsymbol{\mu}_i^j(\boldsymbol{\mu}_i^j)^T \tag{3}$$

where σ_i^j and $\boldsymbol{\mu}_i^j$ are the j-th eigenvalue and eigenvector of $\boldsymbol{K}_i$, respectively; $\boldsymbol{\Lambda}_i$ and $\boldsymbol{U}_i$ are the eigenvalue matrix and eigenvector matrix, respectively. Provided that $\boldsymbol{q}_i^j = \sqrt{\sigma_i^j}\boldsymbol{u}_i^j$, $\boldsymbol{c}_i = [\boldsymbol{q}_i^1, \boldsymbol{q}_i^2, \dots, \boldsymbol{q}_i^r]$, then Eq. (4) can be rewritten as

$$\boldsymbol{K}_i = \boldsymbol{c}_i\boldsymbol{c}_i^T \tag{4}$$

where $\boldsymbol{c}_i$ denotes the stiffness connection matrix of order (n×r), n denotes degrees of freedom. By definition, the baseline global stiffness matrix can be calculated by integration of all element stiffness matrices.

$$\boldsymbol{K} = \sum_{i=1}^{N} \boldsymbol{K}_i = \boldsymbol{CPC}^T \tag{5}$$

where $\boldsymbol{C}$ = [$\boldsymbol{c}_1\boldsymbol{c}_2$,..., $\boldsymbol{c}_N$] denotes the global stiffness connection matrix of order (N×s), $s = r \times N$. $\boldsymbol{P}$ is defined as damage coefficient identification matrix of order (s×s) with all diagonal entries of 1 when no element is damaged, which is given by

$$\boldsymbol{P} = \operatorname{diag}\begin{bmatrix} \underbrace{1-\alpha_1, \cdots, 1-\alpha_1}_{r}, \underbrace{1-\alpha_2, \cdots, 1-\alpha_2}_{r}, \\ \cdots \underbrace{1-\alpha_N, \cdots, 1-\alpha_N}_{r} \end{bmatrix} \tag{6}$$

where α_i denotes damage coefficient of #i element, α_i=0 when no damage occurred in #i element.

Similarly, the change of global stiffness $\Delta\boldsymbol{K}$ before and after damage occurred is given by

$$\Delta\boldsymbol{K} = \sum_{i=1}^{N} \Delta\boldsymbol{K}_i = \boldsymbol{C}\Delta\boldsymbol{P}\boldsymbol{C}^T \tag{7}$$

Substitution of Eq. (7) into Eq. (1) leads to the following form

$$\Delta\boldsymbol{DIL} = \boldsymbol{S}\Delta\boldsymbol{K}^{-1}\boldsymbol{Q} = \boldsymbol{S}(\boldsymbol{C}^{-1})^T(\Delta\boldsymbol{P})^{-1}\boldsymbol{C}^{-1}\boldsymbol{Q} \tag{8}$$

Setting $\boldsymbol{D}$ denotes the transposed virtual inverse matrix of global stiffness connection matrix $\boldsymbol{C}$, $\boldsymbol{L} = \boldsymbol{SD}$, $\boldsymbol{R} = \boldsymbol{D}^T\boldsymbol{Q}$, $\boldsymbol{X} = (\Delta\boldsymbol{P})^{-1}$, Eq. (8) is further simplified into

$$\Delta\boldsymbol{DIL} = \boldsymbol{S}\Delta\boldsymbol{K}^{-1}\boldsymbol{Q} = \boldsymbol{LXR} \tag{9}$$

where

$$\begin{aligned} \boldsymbol{X} &= \operatorname{diag}\begin{bmatrix} \underbrace{\frac{-\alpha_1}{1-\alpha_1}, \cdots, \frac{-\alpha_1}{1-\alpha_1}}_{r}, \underbrace{\frac{-\alpha_2}{1-\alpha_2}, \cdots, \frac{-\alpha_2}{1-\alpha_2}}_{r}, \\ \cdots \underbrace{\frac{-\alpha_N}{1-\alpha_N}, \cdots, \frac{-\alpha_N}{1-\alpha_N}}_{r} \end{bmatrix} \\ &= \operatorname{diag}\left[\underbrace{\lambda_1, \cdots, \lambda_1}_{r}, \underbrace{\lambda_2, \cdots, \lambda_2}_{r}, \cdots, \underbrace{\lambda_N, \cdots, \lambda_N}_{r}\right] \end{aligned} \tag{10}$$

where $\lambda_i = -\alpha_i/(1-\alpha_i)$. The damage coefficient identification problem in Eq. (9) is commonly known as a matrix equation with negative power when the change of DIL before and after damage occurred $\Delta\boldsymbol{DIL}$, with $\boldsymbol{L}$ and $\boldsymbol{R}$ known in advance. Its restricted least-squares iterative solution can be obtained by limiting the value of equivalent damage coefficient α_i in a reasonable range (Zhang *et al*. 2017). In the end, a step-by-step summary of the DIL-based damage detection technique is described as follow:

Step 1: Identification of the DIL before and after damage occurred and calculation of the $\Delta\boldsymbol{DIL}$. According to the positions of unit vertical force on the structure and the selected parts of output DOFs during the DIL identification, the input force selection matrix $\boldsymbol{Q}$ and the output vertical displacement selection matrix $\boldsymbol{S}$ can be obtained.

Step 2: Baseline finite element modeling and updating. The proposed damage extent identification method requires baseline global stiffness matrix and flexibility matrix in bridge health condition, which can be extracted from the baseline finite element model. The damage extent identification accuracy can be affected by the similarity between baseline finite element model and the actual structure. There's been an awful lot of good work done on model updating based on field test data, and the most commonly used model updating indicators including dynamic indicators like model frequency, model shape and static indicators like reflection and strain.

Step 3: Element damage coefficient identification. Decomposing the global stiffness matrix by substituting the obtained stiffness matrix in Step 2 into Eq. (3) and global stiffness connection matrix $\boldsymbol{C}$ can be deduced with Eqs. (4)-(5). Then, the matrix $\boldsymbol{L}$ and $\boldsymbol{R}$ in Eq. (9) could be formed with input force selection matrix $\boldsymbol{Q}$ and the output vertical displacement selection matrix $\boldsymbol{S}$ mentioned in Step 1. Finally, the damage coefficient can be identified by solving the matrix Eq. (9).

2.2 Optimal sensor placement framework

2.2.1 First order sensitiveness analysis of damage coefficients

In the above section, a mathematical model of DIL-based damage detection is established, and the damage extent can be quantified based on the matrix equation defined in Eq. (9). Previous studies have revealed that arbitrary sensor placement could lead to false damage identification (Santi and Sowers 2005). Actually, the performance of the DIL-based damage detection algorithm also depends on the feature of the sensor system, such as the number of sensors and the spatial locations of sensors. To address this issue, an optimal sensor deployment method based on damage sensitivity analysis is proposed in this section.

Eq. (9) described the relationship between equivalent damage coefficient and the change of DIL caused by structural damage, where $\boldsymbol{L}$, $\boldsymbol{R}$ and $\Delta\boldsymbol{DIL}$ can be defined as

$$\begin{aligned} \boldsymbol{L} &= \begin{bmatrix} a_{1,1} & a_{1,2} & \cdots & a_{1,s} \\ a_{2,1} & a_{2,2} & \cdots & a_{2,s} \\ \vdots & \vdots & \vdots & \vdots \\ a_{l,1} & a_{l,2} & \cdots & a_{l,s} \end{bmatrix}, \\ \boldsymbol{R} &= \begin{bmatrix} b_{1,1} & b_{1,2} & \cdots & b_{1,m} \\ b_{2,1} & b_{2,2} & \cdots & b_{2,m} \\ \vdots & \vdots & \vdots & \vdots \\ b_{s,1} & b_{s,2} & \cdots & b_{s,m} \end{bmatrix}, \end{aligned} \tag{11}$$

$$\boldsymbol{\Delta DIL}=\begin{bmatrix} d_{1,1} & d_{1,2} & \cdots & d_{1,m} \\ d_{2,1} & d_{2,2} & \cdots & d_{2,m} \\ \vdots & \vdots & \vdots & \vdots \\ d_{l,1} & d_{l,2} & \cdots & d_{l,m} \end{bmatrix} \tag{11}$$

By substituting Eq. (11) in Eq. (9) and rearranging the matrix $\Delta\boldsymbol{DIL}$ into a column vector by row lead to the following form

$$\begin{Bmatrix} d_{1,1} \\ \vdots \\ d_{1,m} \\ d_{2,1} \\ \vdots \\ d_{l,m} \end{Bmatrix} = \begin{bmatrix} a_{1,1}b_{1,1} & \cdots & a_{1,m}b_{m,1} & a_{1,m+1}b_{m+1,1} & \cdots & a_{1,s}b_{s,1} \\ \vdots & \vdots & \vdots & \vdots & \vdots & \vdots \\ a_{1,1}b_{1,m} & \cdots & a_{1,m}b_{m,m} & a_{1,m+1}b_{m+1,m} & \cdots & a_{1,s}b_{s,m} \\ a_{2,1}b_{1,1} & \cdots & a_{2,m}b_{m,1} & a_{2,m+1}b_{m+1,1} & \cdots & a_{2,s}b_{s,1} \\ \vdots & \vdots & \vdots & \vdots & \vdots & \vdots \\ a_{l,1}b_{1,m} & & a_{l,m}b_{m,m} & a_{l,m+1}b_{m+1,m} & & a_{l,s}b_{s,m} \end{bmatrix} \begin{Bmatrix} \lambda_1^1 \\ \vdots \\ \lambda_1^r \\ \lambda_2^1 \\ \vdots \\ \lambda_N^r \end{Bmatrix} \tag{12}$$

Since the rank of element stiffness matrix r usually greater than 1, there will be several damage coefficients corresponding to the same structural element. However, damage extent of a certain element should be well-determined according to the definition of structural damage, therefore, Eq. (12) is compressed as follow

$$\begin{Bmatrix} d_{1,1} \\ \vdots \\ d_{1,m} \\ d_{2,1} \\ \vdots \\ d_{l,m} \end{Bmatrix} = \begin{bmatrix} f_{1,1,1} & f_{1,2,1} & \cdots & f_{1,n,1} \\ \vdots & \vdots & \cdots & \vdots \\ f_{1,1,m} & f_{1,2,m} & \vdots & f_{1,n,m} \\ f_{2,1,1} & f_{2,2,1} & \cdots & f_{2,n,1} \\ \vdots & \vdots & \vdots & \vdots \\ f_{l,1,m} & f_{l,2,m} & \cdots & f_{l,n,m} \end{bmatrix} \begin{Bmatrix} \lambda_1 \\ \vdots \\ \lambda_p \\ \vdots \\ \lambda_{N-1} \\ \lambda_N \end{Bmatrix} \tag{13}$$

where $\lambda_i = \sum_{j=1}^{r} \lambda_i^j$, $f_{i,p,k} = \sum_{j=(p-1)\times r+1}^{p\times r} a_{i,j}b_{j,k}$ is defined as baseline flexibility coefficient of element #p when unit vertical load applied on node #j and extract the deflection response of node #i. m and l denote input and output degrees of freedom, respectively. $d_{i,j}$ denote the change of DIL in i-th degrees of freedom when unit vertical load applied on node #j.

According to the definition of damage sensitivity, $f_{i,p,k}$ means the sensitivity of vertical displacement output node #i to damaged element #p when unit vertical load applied on node #k. In fact, the position of moving unit load is insignificant in sensitivity analysis, hence, Eq. (13) can be simplified by superposing the change of DIL coefficient under varying moving unit load and rewritten as Eq. (14). The flexibility coefficient matrix is revised accordingly to ensure the consistency of matrix equation.

$$\begin{Bmatrix} G_1 \\ \vdots \\ G_i \\ \vdots \\ G_l \end{Bmatrix} = \begin{bmatrix} F_{1,1} & F_{1,2} & \cdots & F_{1,n} \\ \vdots & \vdots & \ddots & \vdots \\ F_{i,1} & F_{i,2} & \cdots & F_{i,n} \\ \vdots & \vdots & \ddots & \vdots \\ F_{l,1} & F_{l,2} & \cdots & F_{l,n} \end{bmatrix} \begin{Bmatrix} \lambda_1 \\ \vdots \\ \lambda_i \\ \vdots \\ \lambda_n \end{Bmatrix} \tag{14}$$

where $G_i = \sum_{j=1}^{m} d_{i,j}$, $F_{i,p} = \sum_{j=1}^{m} f_{i,p,j}$.

Or

$$\boldsymbol{G} = \boldsymbol{F\lambda} \tag{15}$$

where $\boldsymbol{G} = \{G_1, G_2, \cdots, G_l\}^T$ denotes the change of DIL matrix; $\boldsymbol{F} = \begin{bmatrix} F_{1,1} & \cdots & F_{1,n} \\ \vdots & \ddots & \vdots \\ F_{l,1} & \cdots & F_{l,n} \end{bmatrix}$ is the baseline flexibility coefficient matrix; $\boldsymbol{\lambda} = \{\lambda_1, \lambda_2, \cdots, \lambda_n\}^T$ is the damage coefficient-related matrix.

In order to analyze the sensitivity of DIL to damage coefficient, taking first-order partial derivative of the right side of Eq. (15) with respect to damage coefficient α_i leads to

$$\frac{\partial \boldsymbol{G}}{\partial \boldsymbol{\alpha}} = \frac{\partial \boldsymbol{F}}{\partial \alpha_i}\boldsymbol{\lambda} + \boldsymbol{F}\frac{\partial \boldsymbol{\lambda}}{\partial \alpha_i} \tag{16}$$

Since all the coefficients in $\boldsymbol{F}$ are determined by global flexibility matrix of baseline finite model, the input force selection matrix $\boldsymbol{Q}$ and the output vertical displacement selection matrix $\boldsymbol{S}$, which does not change with damage coefficient α_i, hence, $\partial \boldsymbol{F}/\partial \alpha_i = 0$. In additional, the first-order explicit derivative of damage sensitivity matrix cannot be obtained since the derivative of damage coefficient-related matrix $\lambda_i = -\alpha_i/(1\text{-}\alpha_i)$ with respect to damage coefficient α_i does not exist. Herein, a finite difference method is adopted by adding small perturbations to damage coefficient α_i. The finite difference of Eq. (16) with respect to α_i can be written as follow

$$\frac{\partial \boldsymbol{G}}{\partial \boldsymbol{\alpha}} = \frac{\boldsymbol{F\lambda}(\alpha_i + \Delta\alpha_i) - \boldsymbol{F\lambda}(\alpha_i)}{\Delta\alpha_i} \tag{17}$$

where $\boldsymbol{\partial G/\partial \alpha}$ denotes the damage sensitivity matrix. It is noted that a certain column of $\boldsymbol{\partial G/\partial \alpha}$ represents the sensitivity of an influence line to an element, similarly, a certain row of $\boldsymbol{\partial G/\partial \alpha}$ represents the sensitivity of a displacement node to each element.

2.2.2 Sensor placement based on sensitivity analysis of damage coefficients

To improve the accuracy of damage extent quantification, sensors are expected to be employed in nodes with high sensitivity to structural damage. If the DILs before and after the occurrence of damage in the structure have been obtained, optimal estimate of the damage coefficient matrix $\hat{\boldsymbol{\alpha}}$ can be computed by solving Eq. (17) in a least-square format as

$$\hat{\boldsymbol{\alpha}} = \left(\left(\frac{\partial \boldsymbol{G}}{\partial \boldsymbol{\alpha}}\right)^T \frac{\partial \boldsymbol{G}}{\partial \boldsymbol{\alpha}}\right)^{-1} \left(\frac{\partial \boldsymbol{G}}{\partial \boldsymbol{\alpha}}\right)^T \boldsymbol{G} \tag{18}$$

Since each independent DIL will give different set of $\hat{\boldsymbol{\alpha}}$, Eq. (18) can be modified to include several different DILs. However, it is known that the measured deflection responses are contaminated by measurement noises, which makes it difficult to directly solve the overdetermined set of equations to obtain accurate damage coefficients. In this situation, the effective independence method is adopted herein to solve this problem, in which, the trace of FIM is utilized to evaluate the contribution of each node. The best unbiased estimator of damage coefficient can be obtained when the sum of trace reaches its maximum value in a limited number of sensor. The FIM of node #k can be

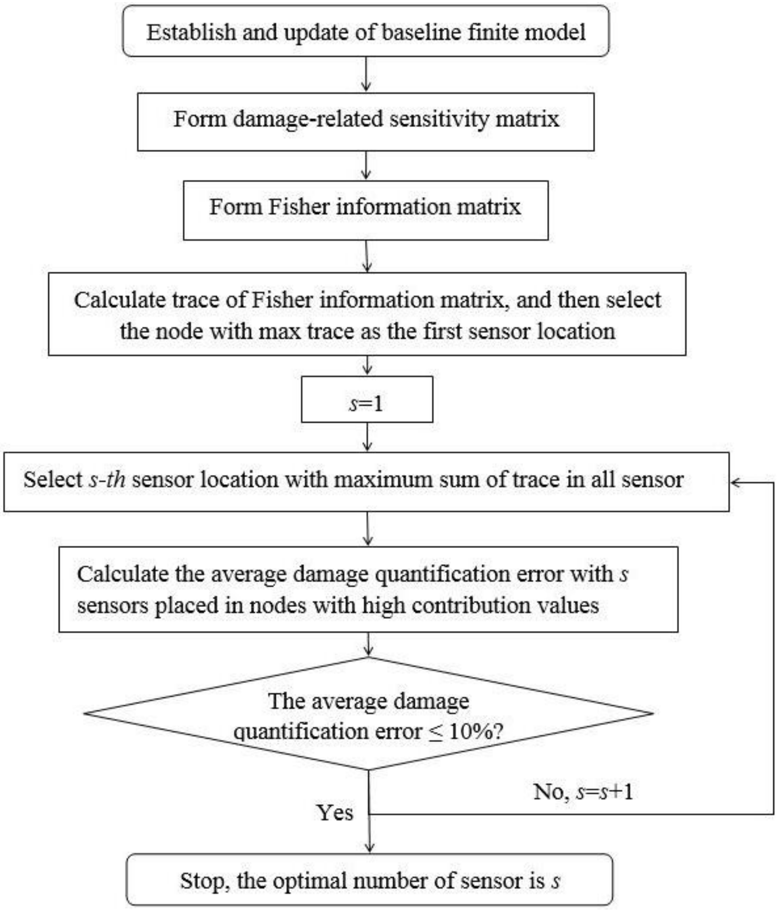

Fig. 1 Sensor optimization process

defined as follow

$$\boldsymbol{A}^k = \left(\frac{\partial \boldsymbol{G}}{\partial \boldsymbol{\alpha}}\right)_k^T \left(\frac{\partial \boldsymbol{G}}{\partial \boldsymbol{\alpha}}\right)_k \tag{19}$$

in which $(\partial \boldsymbol{G}/\partial \boldsymbol{\alpha})_k$ means the corresponding sensitivity matrix of node #k, namely, the k-th row of $\boldsymbol{\partial G/\partial \alpha}$. Even though it is necessary to maximize the sum of trace of FIM to obtain accurate damage coefficients, the redundancy of information should also be taken into account. Otherwise, the selected set of sensors will be overly concentrated and providing damage extent quantification method with repetitive information (He *et al*. 2013).

Euclidean distance is commonly used to evaluate the similarity between matrices. The Euclidean distance between node k and node l can be calculated by following formula

$$d_{kl} = \frac{\sqrt{\sum_{i=1}^{n}\sum_{j=1}^{n}\left|\boldsymbol{A}_{ij}^{k} - \boldsymbol{A}_{ij}^{l}\right|^2}}{d_{max}} \tag{20}$$

where d_{kl} denotes the Euclidean distance between node k and node l, $0 \leq d_{kl} \leq 1$. If the fisher matrix of node k is identical with node l, then $d_{kl} = 0$. $d_{\max}$ denotes the maximum Euclidean distance of any two nodes. In term of the sensing node #k to be chosen, its Euclidean distance respect to all the selected sensing nodes is defined as

$$R_k = min\ (d_{ks}), \forall s \tag{21}$$

where s is the number of selected sensors.

The FIM of node #k in Eq. (21) is rewritten as follow to include the distance coefficient

$$\boldsymbol{A}_k{}' = \sum_{k=1}^{l} R_k \left(\frac{\partial \boldsymbol{G}}{\partial \boldsymbol{\alpha}}\right)_k^T \left(\frac{\partial \boldsymbol{G}}{\partial \boldsymbol{\alpha}}\right)_k \tag{22}$$

To increase the information that have contribution to damage extent quantification, the sum of trace of selected sensor should be as large as possible (Polydorides *et al*. 2018), which can be calculated as follow

$$tr(\boldsymbol{A}') = \sum_{i=1}^{l} tr\left(\boldsymbol{A}_i{}'\right) \tag{23}$$

where $tr(\boldsymbol{A}_i{}')$ means the trace of FIM provided by sensing node #i, and which can be used to evaluate the contribution degree of sensing node #i to damage detection.

It should be noted that each sensing node adds some information to the FIM, but the contribution from each of them is different. Therefore, the candidate sensor set can be selected in terms of their contribution to damage detection. Overall, the above sensor optimization process can be summarized in the following flowchart (see Fig. 1), wherein, the minimum number of sensors s with optimal

Table 1 Beam model properties

Total span length	Linear density	Young's modulus	Section moment of inertia	Damping
30 m	1400 kg/m	2.1×10^9 N/m^2	5.4×10^{-3} m^4	3%

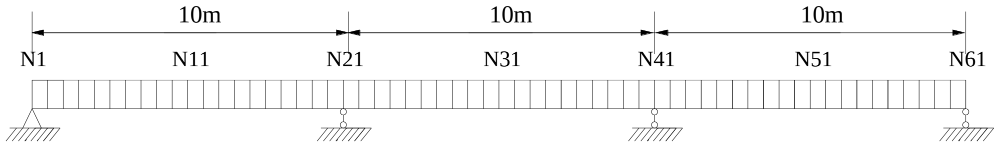

Fig. 2 Three-span continous beam model

placement scheme can be determined when the objective damage quantification error is set in advance. In this study, the optimization goal is set to achieve higher accuracy of bridge damage identification with lesser number of sensors. The actual trade-off should be set by the bridge owner who may consider real application factors such as cost and monitoring requirements. Herein, without loss of generality, the 10% relative damage quantification error is set as a threshold value in advance. Via adoption of the procedure here explained, it is possible to obtain the number and location of sensors and hence optimally design the BHM system.

3. Case studies

Two numerical examples were used to verify the performance of the proposed OSP technique and to define the optimal number of sensors: (1) a numerically simulated, 61-DOF, three span continuous beam with lumped masses on each node; (2) PH bridge with inspected damages. In addition to the verification of the proposed framework, the continuous beam model is used to compare the performance of the distance coefficient corrected damage sensitivity of influence line (DC-DSIL) method to the damage sensitivity of influence line (DSIL) method, and to investigate the effect of different number and location of sensors on damage detection in bridge systems. The real structural damage scenarios from preliminary field inspection result are used for the PH example, and the proposed OSP method is applied to determine priority of sensing locations for a BHM system, which is scheduled to be implemented on the bridge.

3.1 Three span continuous beam

In this section, we use a three-span continuous beam model to illustrates the procedure of the proposed OSP framework and verify its effectiveness. The beam is represented by a finite-element model discretized into 60 beam elements with mechanical properties presented in Table 1. All numerical 3-D models were developed in ANSYS and the analysis was held by the MATLAB. Fig. 2 shows a sketch of the beam in simulation. The structure is assumed to behave elastically, with sensing nodes N1~N61 numbered from left to right.

In order to fully consider the sensitivity of each sensing node to the structural damage, all of the vertical degrees of freedom are chosen herein as output in computing the damage sensitivity matrix. The first-order damage sensitivity analysis is performed according to the rationale introduced in Section 2.2.1. According to the definition of damage sensitivity matrix, a certain column of $\boldsymbol{S}$ represents the sensitivity of a DIL line to an element. Since the beam model shown in Fig. 2 is a symmetrical structure, columns 5, 10, 15, 20, 25, and 30 of the damage sensitivity matrix are extracted and plotted in Fig. 3 to describe the sensitivity of each sensing node to the elements #5, #10, #15, #20, #25 and #30 in the left half of beam model.

In Fig. 3, the absolute maximum value of each sensitivity curve appears in the location of the corresponding element, demonstrating the fact that the closer measurements location to the damage element the more sensitive. As expected, the sensing nodes near the mid-span positions are more sensitive to damage than those near the bearings, indicating that the displacement sensors deployed near middle span are more beneficial to the damage detection, while sensors placed closing to the bearing position are less sensitive to damage detection. It is also observable that the sensitivity values of nodes in side span are relatively higher than those in middle span. Consequently, displacement sensors placed in side-spans are generally more sensitive to structural damage.

Similarly, the sensitivity of selected displacement nodes to each element is analyzed by extracting rows 5, 10, 15, 20, 25 and 30 of the damage sensitivity matrix $\boldsymbol{S}$ and plotted in Fig. 4. It can be seen that there are remarkable peak

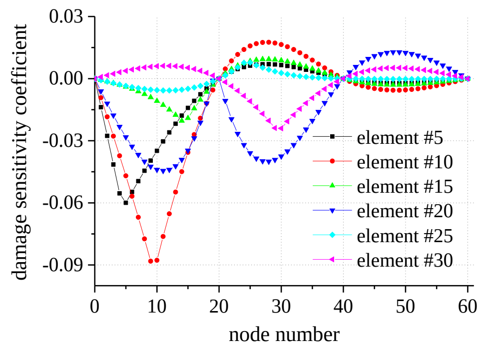

Fig. 3 Damage sensitivity of all sensing nodes to selected elements

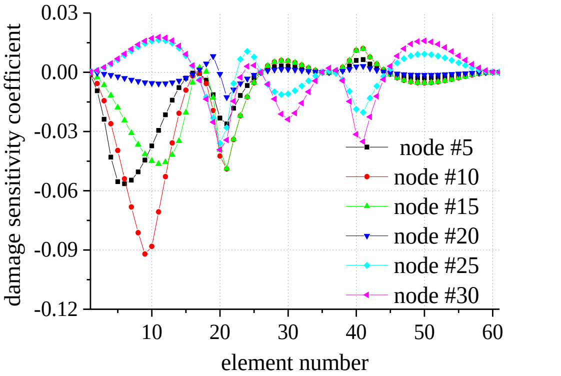

Fig. 4 Damage sensitivity of selected sensing nodes to all elements

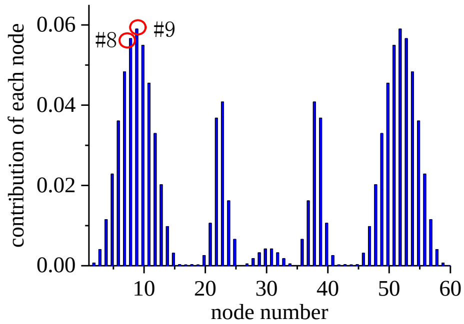

(a) DSIL method

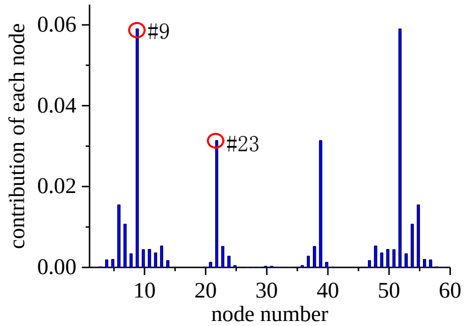

(b) DC-DSIL method

Fig. 5 Contribution of sensing nodes to beam damage detection

values near the bearings (elements #21 and #41, respectively), indicating that the damage occurred near the bearing can be detected if sensors placed properly.

3.2 Comparative study on OSP methods

In above, the damage sensitivity of sensing nodes on beam model is analyzed and then, the contribution of these nodes to damage detection can be evaluated. Fig. 5 shows the contribution of sensing nodes to beam damage detection using the damage sensitivity of influence line (DSIL) method and the distance coefficient corrected damage sensitivity of influence line (DC-DSIL) method described in Section. 2.2.2, respectively.

In the case of DSIL in Fig. 5(a), the contribution of each node is unclear despite there may be cases of peak value (of specific location), which makes it quite difficult to select ideal sensor positions. For instance, if we choose nodes #8 and #9 as sensor positions with respect to the largest contribution value, its normalized Euclidean distances computed from the FIM is only 0.0625. This means that information provided by two adjacent sensors is repetitive and make little contribution to damage detection. However, from the case of DC-DSIL in Fig. 5(b), sensors can be easily placed in node positions with relatively higher contribution, i.e., nodes #9 and #23. Its normalized Euclidean distance is 0.9155, and consequently successfully avoids the information redundancy between enrolled nodes.

The accumulative contribution as the increasing number of sensing nodes calculated by the DSIL method and the DC-DSIL method are compared in Fig. 6, wherein, the accumulative contribution of DC-DSIL method is higher than that of DSIL method. The comparison results illustrate that the DC-DSIL method is quite efficient with respect to the contribution to the improvement of damage detection accuracy. Moreover, the differences are negligible after a certain number of sensors, indicating the sensor placement could be largely optimized aimed at improving the accuracy of damage extent quantification and this has to be taken into account in the design of BHM systems based on displacement measurements.

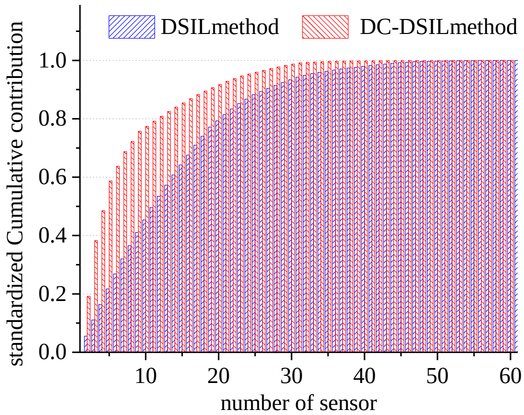

Fig. 6 The number of sensors versus the accumulative contribution

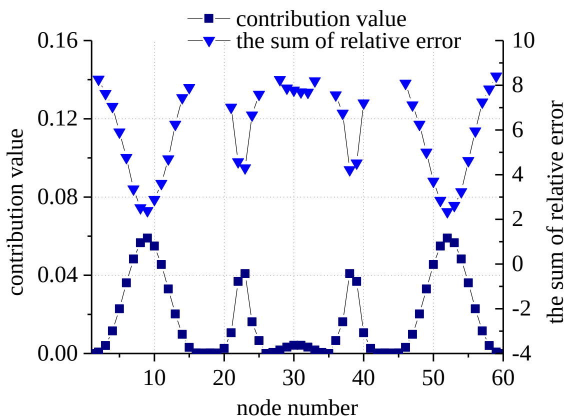

Fig. 7 The sum of relative error and contribution value of each sensing node

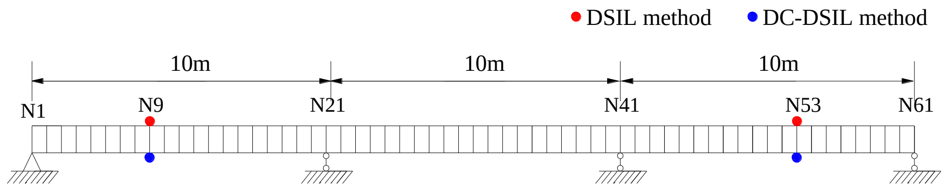

Fig. 8 OSP configurations of two-sensor scheme on the beam

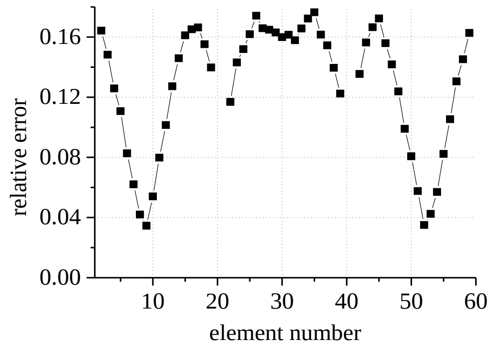

Fig. 9 The relative error of damage detection for two-sensor scheme (sensor placed in nodes #9, and #53; by both the DSIL method and the DC-DSIL method)

3.3 Effects of the number and location of sensors on damage detection

The structural integrity of bridges can be affected by either environmental conditions or unforeseen external actions. In order to efficiently detect damage, a sound sensor deployment scheme should bring accurate detection result to most of damages instead of several special ones. In this direction, we first evaluate the sum of relative error and contribution of every single node to all the elements on the beam. Assuming that damage extent $\alpha_i = 0.2$ is applied to all the elements, and 10% white noise is added to the DIL of each node before and after damage occurred. As evidenced in Fig. 7, the left ordinate denotes the contribution value of each sensing node, and the right ordinate denotes the sum of relative damage quantification error. The inverse relationship between relative error and contribution value of each node is observed in all cases., i.e., the relative errors of nodes #9, #23, #39 and #53 with larger contribution values are apparently smaller than those of others. This phenomenon coincides with the contribution of each node to beam damage detection, and further proves that damage identification is more efficient when nodes with high contribution values are involved in the OSP scheme.

It is worth noting that only one sensor is applied in above discussion. In order to address the effects of number and location of sensors on damage detection, OSP schemes for two (2) sensors and four (4) sensors obtained by the DSIL method and DC-DSIL method are show in Figs. 8-11, respectively. According to the results in Fig. 5, in the case of two-sensor scheme, the peak contribution values occur in nodes #9 and #53. Hence, nodes #9 and #53 are the best positions to place sensors for both the DSIL and DC-DSIL methods. The OSP configurations of two-sensor scheme on the beam structure by both methods are shown in Fig. 8. Fig. 9 shows the relative error of sensors to damage detection when damage extent $\alpha_i = 0.2$ is applied to all the elements, and 10% white noise is added to the DIL of each node before and after damage occurred. The average error of all the damage elements is 12.73%. Moreover, it is obvious that the relative damage quantification errors in element 9 and element 51 are relatively low than those of other nodes, which indicates that damage quantification accuracy can be improved when the damage element is close to the sensor location.

The optimal placement of four-sensor scheme and relative error by both method are shown in Figs. 10 and 11, respectively. When the number of sensors increased from two to four, the standard accumulative contribution value of DSIL and DC-DSIL method (shown in Fig. 5) increase from 11% to 21% and 38% to 59%, respectively. In the case of four-sensor scheme, as shown in Fig. 11(a), the average relative error by the DSIL method decrease slightly to 11.91% when two more sensors in nodes #8 and #54 are enrolled compared to the Fig. 8. Obviously, these two additional sensors do not offer but only marginally to the FIM and thus make little effective contribution to damage detection. By contrast, for the DC-DSIL method in Fig. 11(b), when two more sensors are placed in nodes #23 and #39, the resulted average relative error decrease to 9.36%, which may seem not substantially improved but gives a different sensor configuration. In other words, the DC-DSIL method is able to exclusively detect whether damage occurs on the structure and this is expected to have a direct impact on the optimal sensor positions. As a result, we use the DC-DSIL method in following section to design an OSP scheme for a real bridge. It is note that the average damage qualifica-

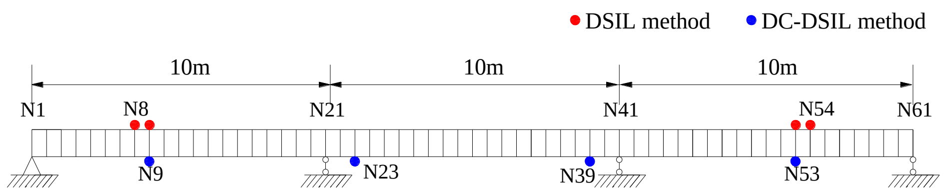

Fig. 10 OSP configurations of four-sensor scheme on the beam

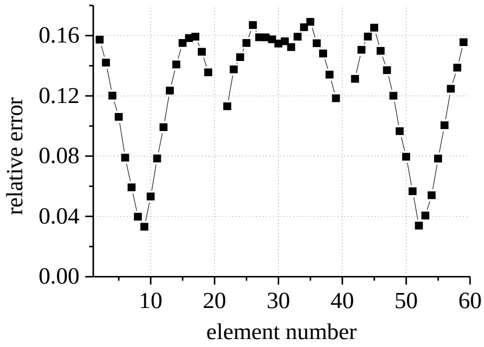

(a) Sensor placed in nodes #8, #9, #53 and #54 by the DSIL method

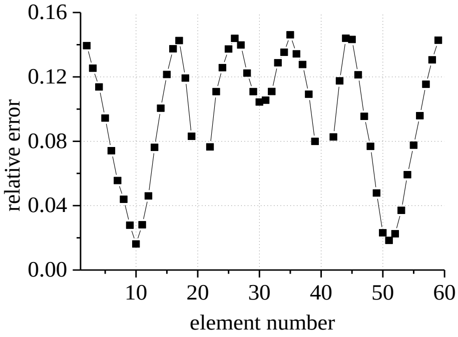

(b) Sensor placed in nodes #9, #23, #39 and #53 by the DC-DSIL method

Fig. 11 The relative error of sensing node to damage detection

(a) Oblique view

(b) Bottom view

Fig. 12 The PH bridge

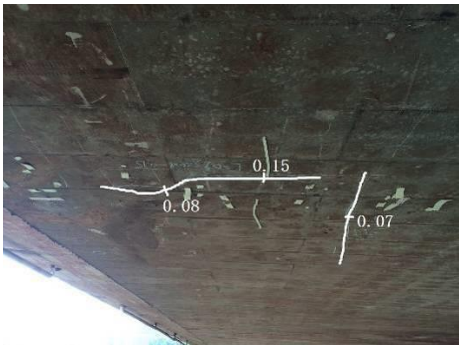

(a) Transverse and longitudinal cracks in bottom slab

(b) Vertical cracks in web

(c) Transverse cracks in bottom slab

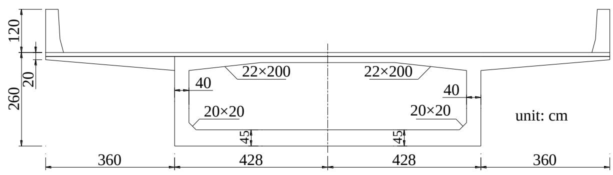

(d) Cross-sectional view of box-girder

Fig. 13 PH bridge deck cross-section and typical structural damages tion error is less than 10% when four sensors placed by the DC-DSIL method. Hence, the optimized four-sensor placement scheme is deemed as sufficient in this numerical study. However, it is also worth to note that such a trade-off should be different case by case, and should be decided based on an overall consideration by the bridge owner at last.

3.4 Pinghu bridge

The proposed OSP approach is adopted in this section to achieve an efficient sensor placement scheme on a field bridge structure. This bridge is currently being retrofitted due to various damages and a BHM system is planned to be implemented to monitor its healthy status in the future. In the following, we present the bridge condition followed by the OSP configuration and its performance evaluation.

3.4.1 Description of the bridge

The Pinghu (PH) bridge pictured in Fig. 12 is located in Shenzhen, China, across the Pinghu railway. It is a four-span continuous reinforced concrete box-girder bridge (42.5 m + 2 × 65 m + 42.5 m). According to its condition inspection in 2015, bridge deck cracks were reported in various locations as shown in Fig. 13 and were set as damage scenarios herein. The location and size of structural damages are summarized in Table 2, where the sizes of damage are represented by the area, respectively. It is note note that the depth of crack is not available in the inspection report, an average depth of 30 cm for cracks therefore is assumed (the web and bottom slab of box-girder have a thickness of 40 and 45 cm, respectively). Then, the stiffness reduction in term of damage area is calculated to estimate the extent of damage in corresponding elements.

The numerical bridge model is divided into 86 elements with equal length. Per the location and size of damage inspected, the bending stiffness losses in corresponding elements are approximately estimated according to the cross-sectional inertia moment before and after the occurrence of structural damage and their damage extent are summarized in Table 2. Fig. 14 gives the discretized bridge model and all of the damage locations, in which, the elements #26, #61 and #75 represent the locations of existing massive cracks respectively. It should be notice that the emphasis of this section is to determine the optimal sensor placement and verify its validity in improving the damage detection accuracy. Hence, some simplification on finite model element division and structural damage scenarios setup are applied herein.

Table 2 The location and extent of typical damages on PH bridge

Damaged element	#26	#61	#75
Damage type	Crack	Crack	Crack
Damage size (m^2)	5.0×0.3	6.0×0.3	6.0×0.3
Moment of inertia before damage occurred (m^4)	1.050×10^9	1.050×10^9	1.205×10^9
Moment of inertia after damage occurred (m^4)	8.925×10^8	8.610×10^8	1.0002×10^9
Damage extent	α_{26} = 0.15	α_{61} = 0.18	α_{75} = 0.17

3.4.2 Sensor placement optimization results

Performing similar optimization procedure, the contribution of all sensing nodes to damage detection are computed using the DC-DSIL method and shown in Fig. 15. As is evident, the first 6 maximum values occur on the nodes #7, #27, #31, #57, #61 and #81, respectively, offering major contribution to damage detection. Therefore, the optimal sensor locations for PH bridge would be selected from those candidate locations in terms of contribution values from high to low. For instance, considering the symmetry of bridge, the magnitudes of contribution values of nodes #31, #7 and # 27 on the left side of bridge are 0.0401, 0.02486 and 0.02464, respectively. Nodes #57, #81 and #61 on the right side have the same values. If only two sensors are decided to be implemented, the sensors #31 and #57 will be selected; if four sensors implemented, extra sensors #7 and #81 will be added; and if six sensors implemented, then extra sensors #27 and #61 will be added. In the present work, we set the number of available sensors at six (6) to simultaneously maximize the information associated with the measurements, and minimize the total cost of the BHM system. Fig. 16 shows the OSP configuration for displacement sensors on the bridge.

Regarding the resulted sensor configuration, Fig. 17 gives an insight into how much the six sensors deployment can detect the actual damages on the bridge (see Fig. 14). It can be obtained from Fig. 17, the relative errors between the identified and real damage extent for damaged elements #26, #60 and #75, are 4.75%, 3.86% and 6.75%, respectively, and the average relative error is 5.12 %. These results prove the damage detection accuracy for the bridge using the proposed OSP framework. Meanwhile, it is also observed that there are some lower peaks others than actual damage locations in Fig. 17, which may cause false positive detection on the bridge. In these cases, the DIL-based methods are shown with errors limiting its damage

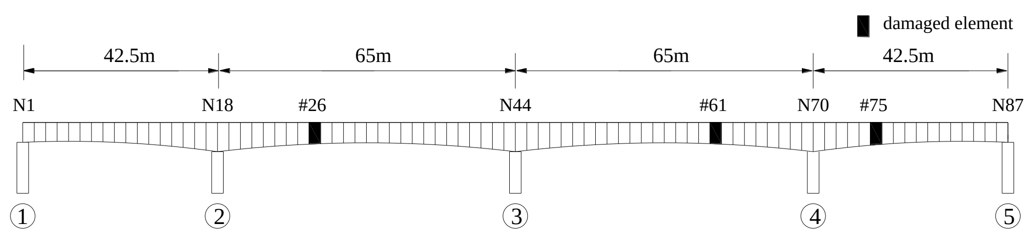

Fig. 14 Damage scenarios and the cross-section of the PH bridge

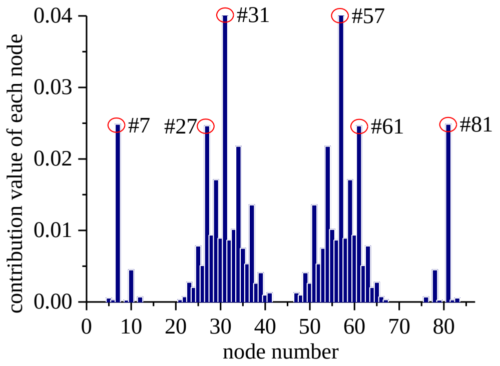

Fig. 15 Contribution of each node by the DC-DSIL method

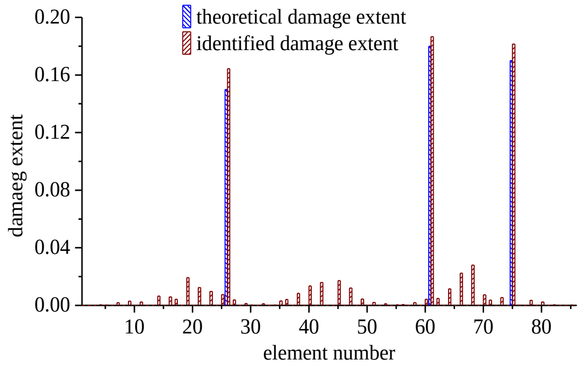

Fig. 17 Damage extent quantification result

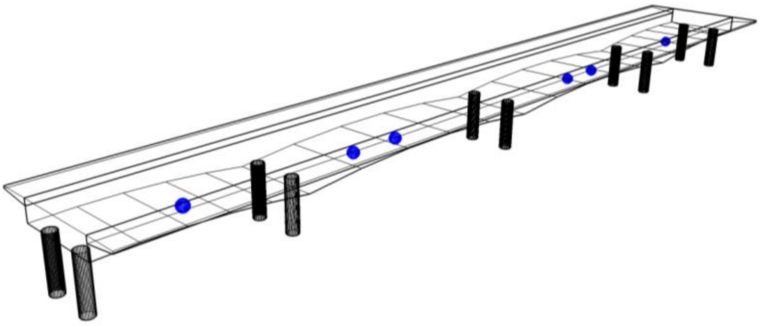

Fig. 16 Optimal displacement sensor configuration for the PH bridge

detection applicability. Overall, this paper offers a methodological approach utilizing displacement sensors via an appropriate and herein developed OSP procedure, in order to derive enhanced estimates of damage based on DIL analysis.

4. Conclusions

In BHM practice, the cost of installing and maintaining of a complicated monitoring system could be a burden to the administration agencies, particularly for those large volumes of existing small and medium scale bridges. Therefore, fewer sensors with efficient placement schemes are deemed as meaningful for real applications. In this paper, our intention is to demonstrate a systematic framework for sensor placement making use of bridge DIL, and to fulfill the damage detection requirements of BHM system. Our method establishes a theoretical connection between the structural stiffness matrix, damage coefficient and change of DIL, and then develops an OSP framework based on the analysis of DIL. The OSP problem has been generalized to take into account the contribution of sensors to damage detection.

The proposed OSP framework allows to quantitatively take into account damage extent detection. Two possible optimization methods have been described, and the relative optimization constraints have been discussed. As results of a three-span continuous beam numerical example illustrate, an inverse relationship between the relative detection error and the contribution to damage detection on each node is observed. Therefore, sensors can be favorably placed on those nodes with higher contribution value to damage detection and thus substantially avoided the information redundancy among enrolled nodes. Moreover, as the number of sensors increase, the DC-DSIL method turns out to be more efficient in damage detection than the DSIL method. It can be explained by the fact that the distance coefficient correction in FIM efficiently improved damage extent quantification accuracy.

From the studies on an actual-scale case study, i.e. the Pinghu bridge, it is observed that, the selected sensor locations show significant contribution in damage detection and, therefore, these locations can be used for potential placement of sensors for practical application of BHM system on this specific bridge. We believe that such a framework can also be used in most of small-medium span continuous bridges. In practice, these sensor locations would serve as an optimization solution for the BHM system to detect structural damages, thus making accurate early-warning of the bridge structure. In the future, similar studies and experimental tests are worth pursuing to make the DIL-based OSP framework more general and applicable to different types of bridges. Meanwhile, to enhance the performance of DIL-based damage detection, displacement records combined with vibration-based measurements featuring higher sampling rates, such as tethered accelerometers and suitable data fusion techniques could be another direction of effort.

Acknowledgments

This work is financially supported by the National Key

R&D Program of China (No. 2018YFC0809606), National Natural Science Foundation of China (No. 51978215), Guangdong Natural Science Foundation (No. 2017A030313290), Shenzhen S&T Projects (No. JCYJ20170811155517130 and GJHZ20180418190651055). The authors are grateful to the authorities for their support.

References

Cavadas, F., Smith, I.F.C. and Figueiras, J. (2013), "Damage detection using data-driven methods applied to moving-load responses", *Mech. Syst. Signal Process.*, **39**(1-2), 409-425. https://doi.org/10.1016/j.ymssp.2013.02.019

Chang, M. and Pakzad, S.N. (2014), "Optimal sensor placement for modal identification of bridge systems considering number of sensing nodes", *J. Bridge Eng.*, **19**(6), p. 04014019. https://doi.org/10.1061/(ASCE)BE.1943-5592.0000594

Chen, Z.W., Yang, W.B., Li, J., Cheng, Q.F. and Cai, Q.L. (2017), "A systematic method from influence line identification to damage detection: Application to RC bridges", *Comput. Concrete, Int. J.*, **20**(5), 563-572. https://doi.org/10.12989/cac.2017.20.5.563

Cho, S., Lee, J. and Sim, S.H. (2018), "Comparative study on displacement measurement sensors for high-speed railroad bridge", *Smart Struct. Syst., Int. J.*, **21**(5), 637-652. https://doi.org/10.12989/sss.2018.21.5.637

Flaga, K. and Furtak, K. (2015), "Examples of solutions for steel-concrete composite structures in bridge engineering", *Civil Environ. Eng. Reports*, **16**(1), 51-68. https://doi.org/10.1515/ceer-2015-0004

He, L.J., Lian, J.J., Ma, B. and Wang, H.J. (2013), "Optimal sensor placement for large space structures based on distance coefficient-effective independence method", *J. Vib. Shock*, **32**(16), 13-18.

Hong, J.C., Kim, Y.Y., Lee, H.C. and Lee, Y.W. (2002), "Damage detection using the lipschitz exponent estimated by the wavelet transform: applications to vibration modes of a beam", *Int. J. Solids Struct.*, **39**(7), 1803-1816. https://doi.org/10.1016/S0020-7683(01)00279-7

Huang, Y.H., Zhu, C.J., Ye, Y.S. and Xiao, Y. (2016), "Damage Detection of Arch Structure by Using Deflection Influence Line", *Proceedings of the 2016 International Conference on Sustainable Energy, Environment and Information Engineering*, Thailand. http://dpi-proceedings.com/index.php/dteees/article/view/4500

Huston, D. (2010), *Structural Sensing, Health Monitoring, and Performance Evaluation*, CRC Press, Boca Raton, FL, USA.

Jin, C., Li, J., Jang, S., Sun, X. and Christenson, R. (2015), "Structural damage detection for in-service highway bridge under operational and environmental variability", *Sensors and Smart Structures Technologies for Civil, Mechanical, and Aerospace Systems*, **9435**, 94353A. https://doi.org/10.1117/12.2084384

Kammer, D. and Brillhart, R. (2013), "Optimal sensor placement for modal identification using system-realization methods", *J. Guid. Control Dyn.*, **19**(3), 729-731. https://doi.org/10.2514/3.21688

Kong, X., Cai, C.S. and Kong, B. (2014), "Damage detection based on transmissibility of a vehicle and bridge coupled system", *J. Eng. Mech.*, **141**(1), 04014102. https://doi.org/10.1061/(ASCE)EM.1943-7889.0000821

Lee, H.S., Hong, Y.H. and Park, H.W. (2010), "Design of an FIR filter for the displacement reconstruction using measured acceleration in low-frequency dominant structures", *Int. J. Numer. Methods Eng.*, **82**(4), 403-434. https://doi.org/10.1002/nme.2769

Li, D.S., Li, H.N. and Fritzen, C.P. (2012), "Load dependent sensor placement method: theory and experimental validation", *Mech. Syst. Signal Process.*, **31**, 217-227. https://doi.org/10.1016/j.ymssp.2012.04.014

Li, H.L., Xia, H. and Guo, W.W. (2013), "Study on mechanism of resonance and vibration cancellation for simply-supported beam under moving loads", *Eng. Mech.*, **30**(7), 47-54.

Li, S.L., Dong, J.L. Lu, W., Li, H., Xu, W.C. and Jin, Y. (2017), "Optimal sensor placement for cable force monitoring using spatial correlation analysis and bond energy algorithm", *Smart Struct. Syst., Int. J.*, **20**(6), 769-780. https://doi.org/10.12989/sss.2017.20.6.769

Liu, H., Qu, W. and Yuan, R. (2003), "Damage detection-oriented sensor optimal placement based on sensitivity analysis", *Earthq. Eng. Vib.*, **23**(6), 85-90.

Liu, X., Pequito, S., Kar, S., Mo, Y., Sinopoli, B. and Aguiar, A. (2013), "Minimum robust sensor placement for large scale linear time-invariant systems: a structured systems approach", *Procedings of the 4th IFAC Workshop on Distributed Estimation and Control in Networked Systems*, Netherlands, January. https://doi.org/10.3182/20130925-2-DE-4044.00067

Loutas, T.H. and Bourikas, A. (2017), "Strain sensors optimal placement for vibration-based structural health monitoring. the effect of damage on the initially optimal configuration", *J. Sound Vib.*, **410**, 217-230. https://doi.org/10.1016/j.jsv.2017.08.022

Mao, J.X., Wang, H., Feng, D.M., Tao, T.Y. and Zheng, W.Z. (2018), "Investigation of dynamic properties of long-span cable-stayed bridges based on one-year monitoring data under normal operating condition", *Struct. Control Health Monitor.*, **e2146**, 1-19. https://doi.org/10.1002/stc.2146

Pei, X.Y., Yi, T.H. and Li, H.N. (2018), "A multitype sensor placement method for the modal estimation of structure", *Smart Struct. Syst., Int. J.*, **21**(4), 407-420. https://doi.org/10.12989/sss.2018.21.4.407

Polydorides, N, Tsekenis, A., Edward F., Chighine, A., Mccann, H., Dimiccoli, L., Wright, P., Lengden, M., Benoy, T., Wilson, D., Humphries, G. and Johnstone, W. (2018), "Constrained models for optical absorption tomography", *Applied Optics*, **57**(7), p. B1-B9. https://doi.org/10.1364/AO.57.0000B1

Santi, L.M. and Sowers, T.S. (2005), "Optimal sensor selection for health monitoring systems", *Proceeding in 41st Joint Propulsion Conference and Exhibit, National Aeronautics and Space Administration*, Glenn Research Center, Tucson, AZ, USA.

Schulte, R., Bohle, K., Fritzen, C. and Schuhmacher, G. (2006), "Optimal sensor placement for damage identification-an efficient forward-backward selection algorithm", *Proceedings of the 3rd European Workshop on Structural Health Monitoring*, Granada, Spain. https://doi.org/10.1002/tal.712

Shi, Z.Y., Law, S.S. and Zhang, L.M. (2000), "Optimum sensor placement for structural damage detection", *J. Eng. Mech.*, **126**(11), 1173-1179. https://doi.org/10.1061/(ASCE)0733-9399(2000)126:11(1173)

Singh, S., Chand, S. and Kumar, B. (2016), "Optimum sink location for sensor deployment in wireless sensor networks", *J. Info. Optimiz. Sci.*, **37**(4), 605-619. https://doi.org/10.1080/02522667.2015.1131025

Soman, R.N., Onoufriou, T., Kyriakides, M.A., Votsisc, R.A. and Chrysostomou, C.Z. (2014), "Multi-type, multi-sensor placement optimization for structural health monitoring of long span bridges", *Smart Struct. Syst., Int. J.*, **14**(1), 55-70. https://doi.org/10.12989/sss.2014.14.1.055

Štimac-Grandić, I. (2014), "Influence of sampling interval on deflection-influence-line-based damage detection in beams", *J. Appl. Eng. Sci.*, **12**(1), 69-74. https://doi.org/10.5937/jaes12-5668

Talebpour, A. and Mahmassani, H.S. (2016), "Influence of connected and autonomous vehicles on traffic flow stability and throughput", *Transport. Res. Part C Emerg. Technol.*, **71**, 143-163. https://doi.org/10.1016/j.trc.2016.07.007

Wang, N.B. and Ren, W.X. (2017), "Extraction of influence line through a fitting method from bridge dynamic response induced by a passing vehicle", *Eng. Struct.*, **151**, 648-664. https://doi.org/10.1016/j.engstruct.2017.06.067

Wang, K.J., Liu, X.L. and Lei, G.U. (2005), "Parallelization of the force method based on generalized inverse matrix in the cluster system", *Chinese J. Rock Mech. Eng.*, **24**(1), 57-65.

Xia, Y. and Hao, H. (2000), "Measurement selection for vibration-based structural damage identification", *J. Sound Vib.*, **236**(1), 89-104. https://doi.org/10.1006/jsvi.2000.2960

Zhang, L., Zhu, A.F., Wu, A.G. and Lv, L.L. (2017), "Parametric solutions to the regulator-conjugate matrix equations", *J. Indust. Manag. Optimiz.*, **13**(2), 623-631. https://doi.org/10.3934/jimo.2016036

BS